CALIFORNIA INSTITUTE OF TECHNOLOGY

DIVISION OF PHYSICS, MATHEMATICS AND ASTRONOMY

PASADENA, CALIFORNIA 91125

HIGH ANGULAR RESOLUTION COSMIC X-RAY ASTRONOMY OBSERVATIONS IN THE ENERGY RANGE 0.15 - 2 keV

and

XUV OBSERVATIONS OF NEARBY STARS FROM AN ATTITUDE CONTROLLED ROCKET

Annual Report: Period 1 September 1973 and 31 August 1974

NASA Grant NGR 05-002-284, CIT XR-5

FINAL

Principal Investigator: Gordon P. Garmire

NASA Technical Officer: Dr. N. Roman, Code SG

Introduction

This report covers the second year effort on this grant to construct a two dimensional focusing Wolter Type I mirror system for X-ray and XUV astronomical observations from an Astrobee F sounding rocket. The mirror design goal will have a one degree field, a 20-arc seconds resolution, and effective area of about 50 cm^2 at 1 keV and 100 cm^2 at 0.25 keV on axis. A star camera will provide aspect data to about 15-arc seconds. Two detectors will be placed at the focus with an interchange mechanism to allow a detector change during flight. One detector is a multiwire position sensitive proportional counter with resolution of about 2- by 7-arc minutes and good efficiency between 0.1 to 2 keV. The second detector is a channel plate multiplier system, with resolution of about 17-arc seconds. It is hoped that the experiment can be flown a large number of times and shared between groups on the west coast at least and possibly with GSFC and Columbia on the east coast. The mirrors and detector system were to be completed during the forthcoming year, but due to recent budgetory limitations, only partial completion of the mirrors may be possible.

The following report is broken down into six sections: I) Position sensitive proportional counter development; II) Channel plate multiplier development; III) Telescope mirror development and payload structure; IV) Australian rocket flights results; V) Comet Kohoutek He I observation; VI) Vela, Puppis A and Gem-Mon bight patch observations.

I. Two Dimensional Position Sensitive Proportional Counter

a) Introduction

To construct a coarse image of an X-ray source, we shall use a two dimensional position sensitive proportional counter in the focal plane of the X-ray telescope. We have made considerable progress during the last year in the development of this detector. The principle of measurement utilizes the rise-time of the pulse for determining the

position of the X-ray event in one dimension (x-direction). For this purpose a wire of high resistivity is used as the anode. The capacitance of the counter together with the high resistance of the anode wire can then be treated as a distributed RC line for the pulse produced on the anode by the incident X-ray. The spatial information is contained in the rise time of the pulses collected at the two ends of the anode. After amplification and pulse shaping, the rise time of the pulses is measured by cross over timing of the bipolar pulses. The delay time of the two pulses is then measured by a time to amplitude counter which then gives a pulse whose amplitude is proportional to the location of the event along the anode wire. The detector is constructed with a number of adjacent cells and the location of the event perpendicular to the direction of the anode wire (y-direction) is determined by the cell in which the X-ray event takes place. The spatial resolution in the y-direction is essentially determined by the spacing of the anode cells. The energy of the incident X-ray is determined by summing the outputs of the two voltage sensitive preamplifiers at either end of the anode wire using a linear adding circuit. A two dimensional position sensitive X-ray counter based on the principle described above has been successfully developed by Borkowski and Kopp at Oak Ridge National Laboratory for hard X-ray application (Borkowski and Kopp, 1968).

b) Test with single cell detector

In order to see whether this type of detector works equally well for low energy X-rays (in .1-2 keV band) we made initial tests with a single anode cell detector which was 50-mm long, 5-mm wide and 5-mm deep. A 0.001" diameter pyrolytic carbon coated quartz filament was used as the anode. This wire has a resistivity of about 8 k Ω/mm. The counter was filled with P-10 gas at one atmosphere of pressure and a

collimated Iron-55 source which produces 5.9 keV X-rays, was used for the initial test run. The size of the spot illuminated by X-rays on the anode was ~ 1 mm. The response of the counter was fairly uniform all along the wire length and typical energy resolution was found to be ≃ 18% FWHM. The position resolution was determined by measuring the pulse height distribution of the time to amplitude converter for 5.9 keV collimated X-ray beam at different places along the anode length. In Figure 1 we have shown pulse height distributions measured at six places on the anode wire. It will be seen from the figure that the typical spatial resolution was about 1 mm and was essentially determined in the present case by the size of the X-ray spot on the anode. In order to see the linearity of response with the position, we have plotted the position of the X-ray source vs. observed peak position of the pulse height distribution in Figure 2. It will be noticed from this figure that the response of the detector is linear with the position within ≃ 3% uncertainty. The detector was then tested with collimated beams of Al-K X-rays (1.49 keV) and sodium K X-rays (1.04 keV). We found typical energy resolution of ~ 32% FWHM and spatial resolution of ≃ 2 mm for Al-K X-rays which was again limited by the area of the anode illuminated by the X-ray beam.

c) Multi-cell position sensitive proportional counter:

Subsequent to the successful working of the single anode cell detector, we have made a multi-anode cell position sensitive detector. The detector had a sensitive area of 5.5 cm x 5 cm and is 5 mm deep. The detector consists of two parts, the main X-ray counter and the veto

counter, for rejecting cosmic ray induced background. The main X-ray counter is made out of a kel-F frame. The detector consists of 14 anode cells, 6 central cells each 2.5 mm wide surrounded on both sides by 4 cells each of 5-mm width. The adjacent cells are separated by 0.010" thick perforated brass strips which sit in the slots machined in the kel-F frame and provide a good ground plane. The anode wire, which is a 0.001" thick pyrolytic carbon coated quartz filament, is fastened to the 0.040" diameter copper tubes epoxied in the frame. A view of the detector system without window is shown in Figure 3. The veto counter consists of 5 anode cells, each 2" long, 0.5" wide and 0.5" deep. The veto detector is mounted behind the main detector and is separated from it by a thin polypropylene window. The anode wires in this counter are also resistive quartz fibers. Both counters are assembled back to back and then mounted in a gas tight box which will also include front end electronics. A 2-μ polypropylene film supported by an egg crate window support collimator serves as the entrance window for the X-rays.

The performance of this multicell detector was initially evaluated using first a 5.9 keV X-ray beam. We consistently obtained energy resolution of $\sim$ 17% FWHM and position resolution of about 1 mm for 5.9 keV X-rays. A schematic diagram of the electronics used in the measurement of energy and position resolution is shown in Figure 4. This electronics set-up is needed for each of the 14 individual cells

of the detector for determination of the position and energy resolution. In order to reduce the electronics requirement by one half we have tried the possibility of linking two adjacent cells to see whether we still get good spatial resolution. In Figure 5 we have shown the results obtained with a 5.9 keV collimated X-ray source. The time to amplitude converter output is plotted in this figure at three different positions of the X-ray source on each of the two linked anode cells. The position resolution is about 2 mm and the concept of linking the adjacent cells seems to work fairly well. We have also carried out the tests with 1.5 keV Al-K X-rays and obtained spatial resolution very similar to that quoted above for single cell detectors. Currently we are evaluating performance of this detector with 0.68 keV Flourine K X-rays and 0.284 keV Carbon K X-rays. We are also investigating the possibility of constructing a parallel plate position sensitive proportional counter similar to the one developed by Mullard Space Science Laboratory in England (Stümpel et al. 1973). The main advantage of this detector is its high spatial resolution in both X and Y directions. It also needs less electronics as only four preamps (and associated electronics) located at four points separated by 90° on the disk are used for determining the position information.

II.a Channelplate High Resolution Detector - Current Status

The operation of the channelplate detector has been described in the two preceding proposals. A schematic diagram of the detector is shown in Figure 6 . Photons or particles enter from the left in this figure and are sensed and amplified in the Chevron microchannel plate A proximity focusing section accelerates the output electron beam towards the aluminum/

phosphor layer. The resulting photon pulse is channeled by the fiberoptics coupling plate and sensed by the self-scanning silicon photodiode array.

From the time of the first conceptual design in January 1972 to the present time, we have built three detector models, and each of these models underwent several minor design modifications. The following summary outlines the development of our design through the various stages of breadboard testing.

Model 1

The initial laboratory detector had low overall gain, and few events were observed on the diode array readout. A Teflon insulator, which was located between the Chevron plate and a flat phosphor/fiber-optics plate, charged up during operation and deflected the emerging electron beam. The phosphor screen was eventually destroyed because the phosphor/aluminum layer burned out along a ring-shaped portion along the periphery. In addition, improper design caused a large number of charged-particle events at the input of the Chevron channelplate.

Model 2

This model was completely successful. The charged-particle rejection, phosphor screen design, and overall gain were all within design values. The results of this experiment have been published ("A High Resolution Position Sensitive Detector for Ultraviolet and X-ray Photons," by G. R. Riegler and K. A. More, IEEE Trans. Nuclear Sci. NS-20, 102, 1973) and are summarized below.

With a 0.053 mm center-to-center Chevron microchannel plate, we observe single-pulsewidths (full width at half maximum of the diode array

image) of, typically, 0.14 mm. Using a diode array with 0.025 mm center-to-center spacing, we can locate the event center to within approximately 0.07 mm. This detector had two sets of particle rejection screens in front of the microchannel plate. However, since the first surface of the microchannel plate was operated at a negative potential of typically -2 kV, it required a comparable bias potential in order to be effective in removing positively-charged ions.

The separation between the output of the Chevron microchannel plate and the aluminum/phosphor layer was 1 mm, and the detector was operated at a bias potential of 4.5 kV. The overall gain predictions deduced from the gain values for the individual components of the system are listed in Table 2. It is apparent that, for the pulsewidth observed on a silicon diode array with 0.025 mm spacing, there exists a gain discrepancy between expected and actual peak charge per diode of a factor of, typically, 4. A similar, although slightly lower, gain discrepancy exists also in our latest detector model, discussed below.

Model 3

The third detector model incorporated the following design changes over the second model: (a) Fabrication for easy interchangeability between 1- and 2-dimensional diode array readout for laboratory analysis purposes, (b) the channelplate/phosphor section can be evacuated while the diode array readout is at atmospheric pressure, and (c) the Chevron channelplate had a center-to-center spacing of 0.017 mm. This model was expected to have a light pulse of 0.080 mm full width at half maximum with an event location definition of approximately 0.030 mm for 0.025 mm diode spacing.

TABLE 2

Summary of Channelplate/Diode Array Gain

Measurements for Two Laboratory Models

Measurement	Model 2	Model 3
Channel center-to-center spacing	0.053 mm	0.017 mm
Chevron microchannelplate gain at 2,000 V (electrons per detected event)	(a) 4×10^6	1.9×10^6
P-20 phosphor gain including fiber-optics input transmittance at 4.5 kV (photons per electron)	(b) 138	(b) 138
Coupling efficiency to the second fiber-optics plate	--	0.82
Fiber-optics plate - diode array coupling loss (oil-free coupling)	0.9	0.9
Total number of photons received on photodiode array	5×10^8	1.9×10^8
Photodiode array geometric efficiency	(c) 0.6	(c) 0.6
Silicon diode detection efficiency at 5,600Å (electrons per photon)	0.68	0.68
Total charge expected (Coulomb)	3.3×10^{-11}	1.3×10^{-11}
Observed event width (full width at half maximum for light distribution)	0.125 mm = 5 diodes	(d) 0.2 mm (prelim) = 8 diodes (prelim)
Peak diode charge Q_m predicted (Coulomb)	6.5×10^{-12}	(d) 1.5×10^{-12} (prelim)
Peak diode charge Q_o observed (Coulomb) based on saturation charge of 2×10^{-12} C quoted by manufacturer	1.6×10^{-12}	(d) 0.5×10^{-12} (prelim)
Gain discrepancy factor	4	3

Notes:

(a) Low-gain sample supplied by Bendix Electro-Optics Division.

(b) Actual measurement by the Bendix Electro-Optics Division was 166 photons per electron at 5 kV bias potential, P-20 on fiber-optics plate. The value shown was scaled for 4.5 kV, allowing for 2 kV "dead" voltage. Other values, lower and higher by approximately 20%, are obtained when various other published values for the phosphor conversion efficiency are used.

(c) The linear photodiode array used here has an effective width of 0.015 mm on 0.025 mm spacing.

(d) The event width quoted here is a preliminary value. Modifications to proximity-focusing section and other portions of detector are expected to reduce event width. However, total amount of light received is not likely to change, so that gain discrepancy may still remain.

A view of the complete laboratory assembly is shown in Figure 7 A tubing/valve assembly was used for temporary connection to a vacuum station in order to keep the inside of the assembly as clean and dust-free as possible. During actual operation inside a vacuum system, the front plate is removed so that the restriction caused by the small 1/4-inch tube is eliminated. The high voltage feedthroughs were made of Kel-F and were designed for a corona voltage in air of approximately 10 kV. This design is very conservative for most vacuum-system applications since we usually place the output of the microchannel plate at ground potential, and the phosphor bias potential is usually limited to from 5 to 6 kV.

Table 2 contains a summary of the gain measurements for this detector system. As for Model 2, we find that there exists a difference between expected and actual observed peak gain per detected event. This difference underlines the need to design any new systems with sufficient gain reserve to obtain saturation or near-saturation events, even with some gain degradation during the life of the detector.

The presently observed pulsewidth for this latest detector model is broader than expected, as indicated in the table. It is, of course, possible to define the event center to within, typically, 0.05 mm from an analysis of the signals from all diodes around the event center. However, this requires more bits of data information and is less accurate than in the case of narrower pulsewidth. We believe that the pulse spreading is primarily caused by an excessively large separation between the microchannel plate output and the phosphor screen, as well as by slight surface irregularities in our present detector, which result in field-shape distortions. We are

currently planning to modify the whole region surrounding the proximity-focusing section between the microchannel plate output and the phosphor screen in order to reduce the pulsewidth to the expected value of 0.080 mm FWHM. In addition, the coupling between the two fiberoptics plates has been modified in order to reduce any beam spreading at that interface.

TABLE 3

Survey of Quantum Efficiency

Measurements

Line	Energy keV	Wavelength A	Quantum Efficiency	Angle W.R.T. Surface	Material	Device	Reference
O	.0095	1304	.002	20	Glass	S	LAB
M	.0102	1216	.009	20	Glass	S	LAB
			.023	20	Glass	S	LT
			.010	90	MgF_2	S	LT
H_2	.0136	906	.084	20	Glass	S	LAB
			.12	90	MgF_2	P	LT
			.15	90	LiF	P	LT
Ne	.0167	794	.14	20	Glass	S	LAB
He	.0212	584	.13	20	Glass	S	LAB
			.13	20	Glass	S	LT
			.36	20	MgF_2	S	LT
			.37	45	MgF_2	P	LT
Ne	.027	461	.13	20	Glass	S	LAB
			.09	20	Glass	S	LT
			.23	20	MgF_2	S	LT
He	.041	304	.13	20	Glass	S	LAB
C	.282	44.7	.08	20	Glass	S	LAB
			.09	20	Glass	S	SP
			.057	4	Glass	M	HEAO-B 9-73
			.25	4	Glass	M	HEAO-B 12/73
Al	1.5	8.34	.046	20	Glass	S	LAB
			.05	20	Glass	S	SP
			.042	4	Glass	M	HEAO-B 9-73
			.13	4	Glass	M	HEAO-B 12-73
			.38	30	CsI	P	TS, Luk.
			.85	10	CsI	P	TS
			~ .9(expect)	90	NEAD		HEAO-B 9-73
Va	4.5	2.75	.21	90	NEAD		HEAO-B 9-73
Fe	5.9	2.1	.023	20	GLASS	S	LAB

Explanation of table entries:

Glass = standard lead-doped, activated glass photoemissive surface

NEAD = negative electron affinity detector surface

S = single-channel device, e.g., spiraltron electron multiplier with cone aperture

M = multi-channel device, e.g., microchannel plate

P = flat photocathode with separate electron collection and amplification

References:

LAB = Our laboratory measurements, conducted 1971 - 1973

LT = Lapson, L.B., and Timothy, J.G., "Use of MgF_2 and LiF Photocathodes in the Extreme Ultraviolet", Appl. Optics 12, 388, 1973

SP = Smith, D. G. and Pounds, K. . 1968, Trans. of IEEE, NS-15,No 3,541.

HEAO-B 9-73 = "The HEAO-B X-ray Observatory", Report prepared for OSS special review, 13-14 September 1973, Consortium headed by R. Giacconi, Center for Astrophysics, September 1973

HEAO-B 12-73 = Monthly Progress Report, The HEAO-B Consortium, December 1973

TS = T. Somer, "Soft X-ray Detectors", Bendix Research Laboratories Technical Report AFML-TR-68-188, July 1968

Luk = Lukirskii, A.P., Rumish, M.A., and Karpovich, I.A., "Measurement of the photoelectric yield of the external photoeffect under the action of X-rays in the wavelength range 1.54 - 13.3 A", Optika i Spektroskopiya 9, 653, 1960

II.b Survey of alternate high-resolution detector concepts

New solid-state image sensors

The high-resolution channelplate detector described in Section 3.5 uses a phosphor screen to convert the electron beam of 10^6 to 10^7 electrons per photon into visible light. This visible image is then analyzed by a self-scanning silicon diode array. Photons give rise to electron-hole pairs within each silicon diode; the electrons move to the anode, while holes become trapped and reduce the net charge on the diode. During the next periodic scan of the diode, the amount of current required to charge the diode up to the nominal value is amplified and represents the signal.

The recent developments among solid-state photon sensing devices include the charge-coupled (CCD) and charge-injection (CID) device. Like the silicon diode array they are based on silicon solid-state sensors and are read out by various charge transfer schemes without the use of an electron beam. However, these devices are still in the prototype or custom-order stage and are both more expensive and less reliable than the Reticon diode arrays. However, the situation is expected to reverse within approximately 2 - 3 years, and we may at that time consider a change in the readout scheme.

II.c Direct electron image sensing

Instead of converting the electron burst from the channelplate into a visible image, one might consider eliminating the conversion and using an electron image sensor. The self-scanned diode array cannot be used as electron sensor since the protective SiO_2 layer on top of the silicon would charge up and cause distortions or damage in the proximity-focusing region.

Although this concept has been used for very low light-level images, it cannot be employed at the electron concentrations encountered in our device.

The charge-injection device mentioned in Section 3.4.1 above should, at least in principle, be able to withstand electron burst impacts since manufacturers claim that they do not need to deposit an insulating SiO_2 layer on the silicon wafer. In addition, it might be possible to achieve amplification within the silicon wafer if the electrons from the channelplate are accelerated to high energies. For example, a 20 keV electron should produce approximately 6700 electron-hole pairs if 3 eV are required to generate an electron-hole pair. This concept would even allow us to eliminate the first channelplate in the Chevron plate device.

This concept will be studied in more detail and verified experimentally when suitable CID's become available. However, we are not currently planning studies of this type since neither the X-ray detection efficiency nor the readout characteristics differ from the present detector.

II.d Separate photocathode devices

II.d.1 Negative electron affinity detector

In this type of detector, a dipole layer at the photocathode surface lifts the electron conduction band above the energy of the external vacuum, and escape of electrons is more likely than in standard materials. As a result, high detection efficiencies approaching 100% are possible. This type of photocathode can be operated in either the "reflection" (opaque photocathode) mode or in the transmission mode. The electron signal in either device must be electromagnetically focussed to an electron sensor/amplifier, e.g., phosphor and image intensifier. A disadvantage of the

negative electron affinity detector is that the low-energy X-ray response at less than approximately 0.5 keV is severely reduced because of the deadlayer required on the current GaAs photocathodes.

We are following this development, but are not currently involved in any laboratory studies of the negative electron affinity detectors.

II.d.2 Oblique photocathode detector

This device uses the usual method of sensing the photoelectrons from an opaque photocathode. The direction of motion of the secondary electrons is essentially opposite to that of the incident photons. In particular, electromagnetic focusing generates an oblique angle of typically 150^{o} between the photon and the secondary electron directions. There are two advantages which make this scheme attractive for certain applications: (a) The photocathode can be readily interchanged to provide X-ray, far ultraviolet, ultraviolet or visible-light response without any loss in spatial resolution, and (b) the electromagnetic focusing section can be designed for 1:1 image size transfer or for magnification or reduction up to a factor of 5 (factors up to 10 may be feasible). A prototype device for ultraviolet light imaging has been built and tested successfully at the Bendix Research Laboratories.

The use of the oblique photocathode detector with a negative affinity photocathode and other photocathodes may be of interest to this experiment at a later stage. However, we are not planning to use this detector approach for the first two rocket flights.

II.e Summary of detection efficiency measurements

Efficiency of the X-ray telescope and the detectors has been shown as a function of energy in Figure 8. During the past few years we have carried out a number of quantum efficiency measurements in the extreme

III. Telescope Fabrication

Last year we were told at the project initiation meeting at GSFC that an Astrobee F rocket has been assigned for the first flight of the focusing telescope experiment. This rocket has a 17" diameter cylinder. In order to take advantage of this extra available space, we modified the design of the mirrors and increased the diameter of the outer mirror to 15" and that of the nested inner mirror to about 12".5. The lengths of the mirrors were, however, kept the same (10".5) due to limitation on the capability of the precision machining lathe at Oak Ridge Y-12 plant. A new design of the X-ray telescope is shown in Figure 9.

Rough machining of the new outer paraboloid and hyperboloid mirrors from forged aluminum blocks was first done in the Caltech shop. The surfaces of the two mirrors were then further machined to a precision of $\sim$ 0.3 mil to make the required paraboloid and hyperboloid contours. For precision machining the paraboloid mirror was sent in early January to the Oak Ridge Y-12 plant. Prior to machining a 0.001" thick layer of copper was deposited on the surface of the mirror. The copper surface was then machined on the precision lathe at the Y-12 plant. From measurements of the machined surface of the paraboloid at Oak Ridge we are told that the peak to valley amplitude of the irregularities on the surface is about 32 microinches. This is about a factor of three higher than what was expected. The main source of error seems to be due to the vibration of the mirror holding fixture on the lathe. This is the first time that a mirror of this size has been machined at the Y-12 plant.

The Y-12 plant engineers now feel that in light of their experience with this mirror, they will be able to provide a better surface finish on the next set of mirrors. Subsequent to machining, the copper surface of the paraboloid mirror was coated with electroless nickel. We have received the mirror recently and have evaluated its surface. A photograph of the paraboloid mirror is shown in Figure 10. The surface was unacceptable, but a new machining with a better damping fixture will be attempted. In coming months we propose to finish the precision machining of the hyperboloid mirror at the Y-12 plant and rough machining of the nested mirrors in the Caltech shop.

III.a Lapping the Mirror Surface

After precision machining and deposition of the electroless nickel, the mirror surface has to be suitably lapped to smooth out surface irregularities produced during the machining. These surface irregularities are essentially high spatial frequency deviations of the order of 15 microinches which have a correlation length of about 100 microinches or less. These arise mainly from the mechanical vibrations and the tool stroke during the machining. Since reflection properties of the mirror depend very critically on the smoothness of the reflecting surface, the polishing of the mirror surface has to be done very carefully. During the past year we have been trying various polishing techniques for lapping the surface of a 14" diameter paraboloid mirror which was fabricated for the Aerobee vehicle. We have been trying the polishing process at different values of lap pressure, lap speed and rotation rate of the mirror to determine the optimum values of these parameters. Linde "B" powder, which has particles of 0.05 micron size is being used as the abrasive in the polishing process. The results are so far not conclusive. We are also investigating the

feasibility of using a submerged polishing process which has been successfully used at AS & E for polishing quartz mirrors.

III.b Payload structure

Rationale for an evacuated payload structure

The major parameters of the rocket payload structure have been finalized and correlated with the GSFC Sounding Rocket Branch. The vehicle to be used is an Astrobee F with 17.256 in. outer diameter. The payload section is now set at 100 in. overall length. The baseplate has a 5 in. high shoulder onto which the 95 in. long extension skin is mounted. The 5 in. high section contains all pull-away and ground support equipment connectors. Mechanical layout of the payload is shown in Fig. 10.

Experience with the various laboratory models of the channelplate high resolution detector (see Section 3.5) has shown that high vacuum around the detector is an important requirement. Although the detector can operate at 10^{-5} Torr, the possibility of damage to either the channelplate or the phosphor screen sections is quite high. Satisfactory operation has been achieved repeatedly at pressures of approximately 2×10^{-5} Torr or less. At this pressure, a faint glow on the phosphor screen (which appears at higher pressure due to trapped-gas ionization near the interface between the two channelplates, and does not have enough overall gain to be visible on the diode array) disappears, and a background rate of events of typically 1 - 5 events/cm^2-s is observed.

During a sounding rocket launch, the ambient pressure varies from 1 atm to less than 10^{-6} Torr within approx. 1 minute. However, the pressure near a detector inside a payload does not decrease as rapidly as the ambient pressure mainly as a result of outgassing of the large skin and payload structure surfaces. Water vapor trapped in surfaces is the single most persistent source of residual gas. Launch simulations carried out at MSFC by the Harvard Observatory group (Timothy, 1973) showed clearly that residual gas on the channel surface and on ambient surfaces results in counting rate distortions. The detector used by this group was a single-channel device; the outgassing problem should therefore be even more severe for the microchannel plate device to be used in our experiment.

Both of the difficulties described above can be circumvented by the following payload modification. This modification has been discussed with the GSFC Sounding Rocket Branch and has been accepted as the design baseline. Prior to launch, the whole experiment payload extension will be evacuated to a pressure of 10^{-4} Torr or less. The vacuum line to the appropriate vacuum pump on the launch tower will be closed off by a commandable valve 10 s prior to lift-off. This approach will assure a minimum of trapped gas on the extension can surface and the experiment surfaces. It is worth pointing out that <u>all</u> extension cans for Astrobee Black Brandt payloads are being constructed with O-ring grooves since many new payloads are being designed for evacuation prior to lift-off.

In addition to the experiment section evacuation, the high resolution channelplate detector is located in a high-vacuum box with a 2 l/s ion pump attached. This ion pump will be powered on the ground through an external connector. The high-vacuum box will be kept at a pressure of 10^{-6} Torr or lower. The current plan calls for a bakeout at 80 - 100 C in the laboratory, with subsequent pumpdown to 10^{-4} Torr by an external vacuum pump. The ion pump is then activated for pumpdown to less than 10^{-6} Torr. Unless any maintenance is required, the high-vacuum box will reamin closed and evacuated throughout transportation to the WSMR and the pre-launch checkout sequence there.

The cover plate for the high-vacuum box can be opened and closed on command. The actuating mechanism is almost identical to that used for the HEAO A-2 Low Energy Detector protective cover, except that the parts used have standard industrial quality. A total of four timer functions (1 primary and 3 back-up functions) are used to make sure that the box cover will open properly.

IV) Australian rocket flights results

The detector system for both CIT flights consisted of four proportional counters, three of which were devoted to the low energy observations and were covered by carbonized 1.5-micron polypropylene windows and filled with propane gas at 150 torr. The fourth detector was filled with P-10 gas at 810 torr and covered by a 13-micron mylar window.

The detector collimation, detector area and energy range above 10% efficiency are given in Table 1. The approximate detection efficiency

of detectors A through C is shown in Figure 1.

Table I

Detector	Area	Collimation	Energy Range
A	250	$0.4^{\circ} \times 10^{\circ}$	0.15 - 3.0
B	250	$2^{\circ} \times 10^{\circ}$	0.15 - 3.0
C	350	$5^{\circ} \times 10^{\circ}$	0.15 - 3.0
D	350	$10^{\circ} \times 5^{\circ}$	1.2 -12.0

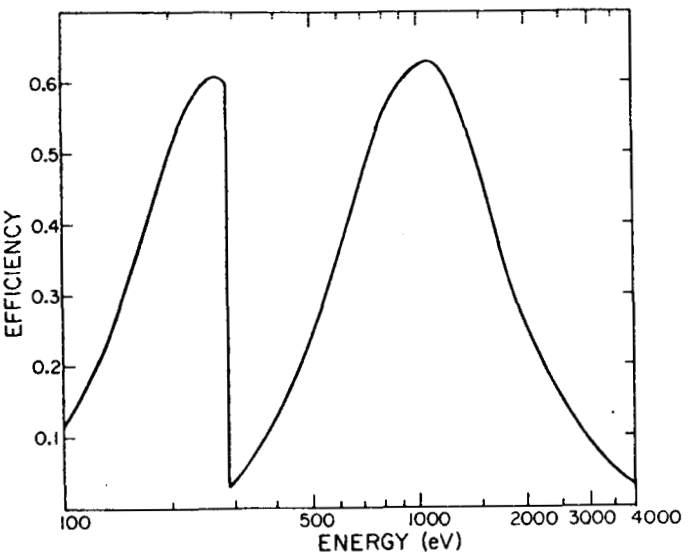

Figure 1

Cen X-3

The first source studied was Cen X-3, which was scanned on both flights. The first observation was for 35 seconds. Pulses were observed in the P-10 detector at the 4.8 sec period observed by Schreier et al. (1972). The spectrum is quite hard (KT ~15 keV) and no low energy excess was observed in contrast to an earlier report by Bleeker et al. (1973). Figure 2 shows the comparison. The orbital phase during the observation

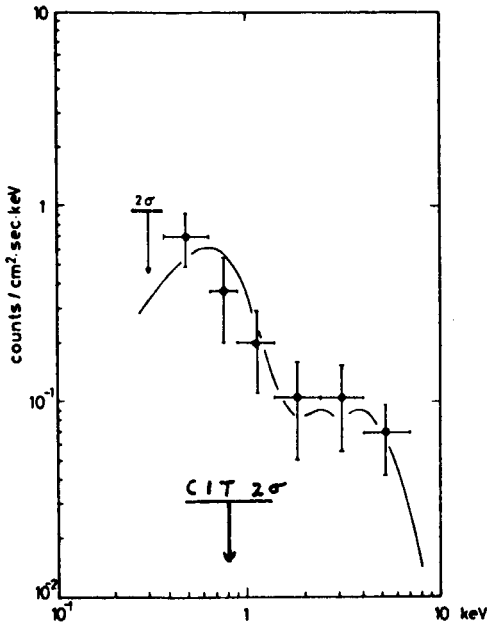

Figure 2

was about 0.2. In view of the optical data by Vidal et al. (1974) which gives a distance of between 5-10 kpc and E(B-V) of 1.36 which gives a value for N_x (equivalent H-atoms/cm^2) of 10^{22} (Ryter et al., 1974), it is not surprising that no flux was observed near 1 keV. Bleeker and collaborators must have detected a soft source of emission near Cen X-3, unlikely as it seems, which must have been transient since such a bright source would have been easily detected by our scan unless it lay at some distance from Cen X-3 along Bleeker and associates' collimator which extended for about 12.5^{o} on either side of Cen X-3.

The second flight took place during the eclipse portion of the binaries' orbit and no detectable flux above our noise limit of about 0.03 photons/cm^2-sec was observed. In the eclipse position the observations of Schreier et al. (1972) show occasionally a positive result of

about 0.02 ph/cm^2-sec in the 2-6 keV band. This is about our upper limit for this particular eclipse.

Vela X-1 (3U0900-40)

This source was observed on 9 November for about 20 seconds. It is identified with the star HD 77581 and is estimated to be quite massive (Wickramasinghe et al., 1974), possibly more massive than a neutron star. It has a period of 8.95 days and is at a distance of about 2 kpc. The data obtained by the D counter on the flight of 9 November corrected for aspect variations is shown in Figure 3 at a time resolution of 0.25 seconds. The basic resolution of the recording system is 1.6 m sec, but

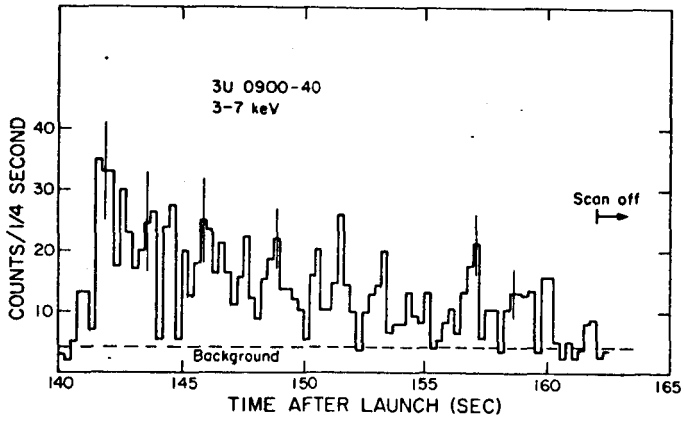

Figure 3

the source intensity is too low to obtain significant results in this short a time interval. During the observation the source strength falls by nearly a factor of two. In addition, rapid flickering on a 0.25 second time scale is observed. A power spectrum analysis and search for bunching of pulses (shot noise) has not been completed. The source is

clearly noisy on all time scales observed by this experiment, which implies a quite compact source (of order 10^{10} cm or less).

3U 0614 + 09

The source 3U 0614 +09 (Giacconi et al., 1974) was observed on 9 November by the D counter. The intensity in the (2-7) keV band is 0.2 ph/cm^2 sec and the spectrum is softer than either Vel X-1 or Cen X-3. The source varies by a factor of six which is much greater than the observed variation of Sco X-1 (Giacconi et al., 1974), a source which has been compared to 3U 0614 +09 by Murdin et al. (1974). The optical candidate identified by Murdin and collaborators at a blue magnitude 18.5 compares well with Sco X-1 scaled by the X-ray intensity.

η Car

The region of η Car was observed on both of the CIT flights. No source was detected at the position of η Car, although a possible soft source was observed nearby which exhibited time variations on a scale of seconds. The properties of this source will be reported later. The upper limits to η Car in two energy bands are:

$$J_x\ (\tfrac{1}{4}\ \text{keV}) \leq 0.03\ \text{ph/cm}^2\ \text{sec}$$

$$J_x\ (1\ \text{keV}) \leq 0.04\ \text{ph/cm}^2\ \text{sec}.$$

This compares to the reported flux of 0.23 c/cm^2 sec reported by Hill et al. (1972) for a source near η Car. We did not see any flux at their reported most likely source position, some three degrees from η Car. The source in this region must be variable. No known U-Gem type star is near this position.

LMC

The LMC was scanned for about 140 seconds during the flight of 1 November. The scan path is shown in Figure 4. We find a general emission from the entire region of

$$J_x \text{ (3-7 keV)} = 0.18 \pm 0.06 \text{ ph/cm}^2 \text{ sec}$$

$$J_x \text{ (0.5-1.5 keV)} = 0.1 \pm 0.025 \text{ ph/cm}^2 \text{ sec}$$

$$J_x \text{ (0.1-0.4 keV)} \leq 0.2 \text{ ph/cm}^2 \text{ sec}$$

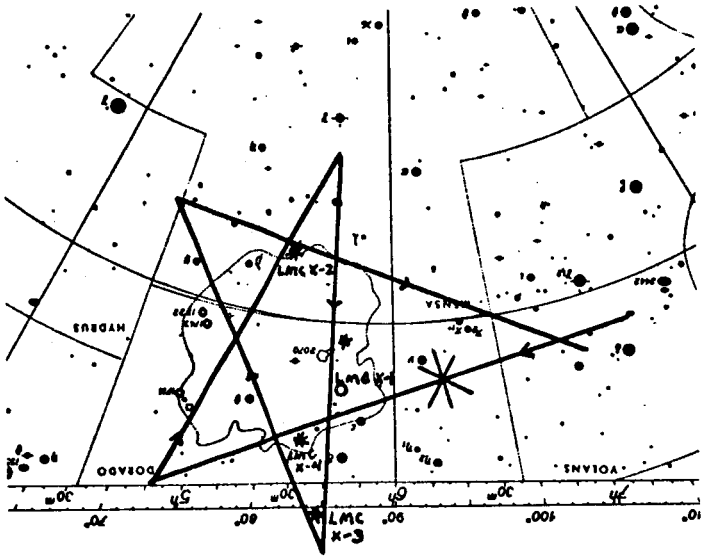

Figure 4

The spectrum of Price et al.(1971) is shown in Figure 5 for comparison. The lack of flux at 1/4 keV is consistent with a column density of hydrogen equal to about 6×10^{20} atoms/cm^2.

Dr. S. Rappaport of MIT reports that they detected a flux of 0.5 - 1.0 keV photons apparently emitted from the bar of the LMC barred spiral configuration. The peak of their flux was about 10' from the center of the bar and 33' from the source LMC X-1. The MIT flux was estimated to be

$$J_x\ (0.5 - 1.0) \approx 0.4 \pm 0.07\ \text{ph/cm}^2\ \text{sec.}$$

This flux is greater than the flux observed by CIT by more than the estimated errors, so that a more detailed analysis will be required to resolve this discrepancy.

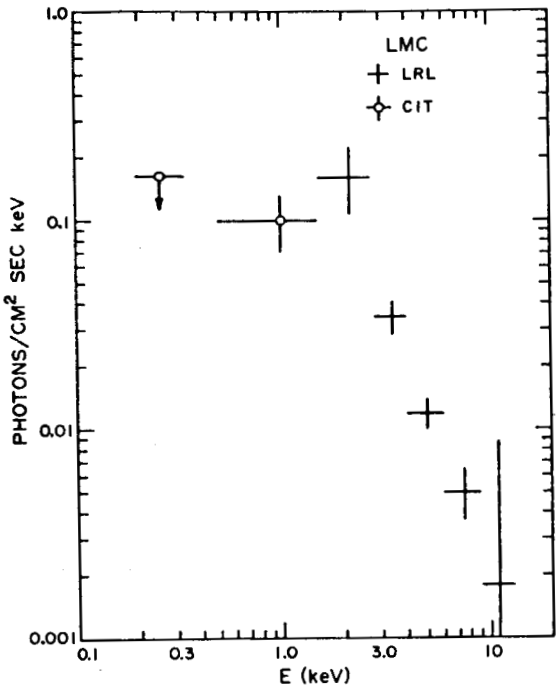

Figure 5

The observed flux (CIT), if assumed to originate from the region of the optical nebula, corresponds roughly to the surface brightness of the north galactic pole. Whether the emission originates in a collection of discrete sources or a diffuse emission process can not be answered at this time. The emission is relatively faint and may be from an oval or bar shaped region in that MIT failed to detect the emission while scanning along the bar, but saw it when their long, narrow field of view passed over the bar.

Mon-Gem and Eridanus Regions

The Eridanus region was scanned on the 9 November flight for spatial structure and spectral properties. The emission region and scan path are sketched in Figure 6 and the counting rate as a function of time

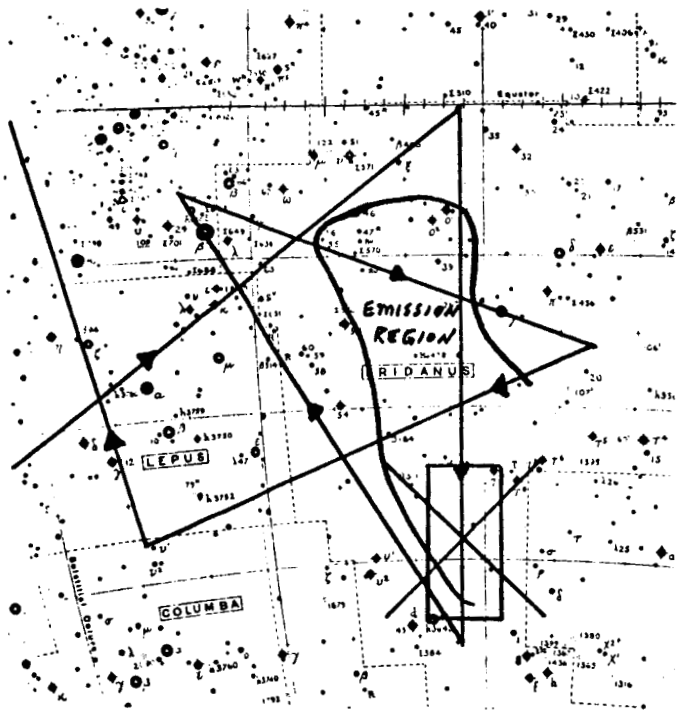

Figure 6

is shown during the scan for the 5^{o} x 10^{o} FoV detector and the 2^{o} x 10^{o} FoV detector in Figure 7. The bulk of the emission appears to come from a diffuse emission rather than a few point sources. Numerous (> 5) point sources cannot be ruled out.

The Mon-Gem region was scanned on a previous flight on 24 March 1973 and the spectrum obtained is shown in Figure 8. The temperature was about 3 million degrees, although the range of possible temperatures and absorption values is large. These emission regions could be the

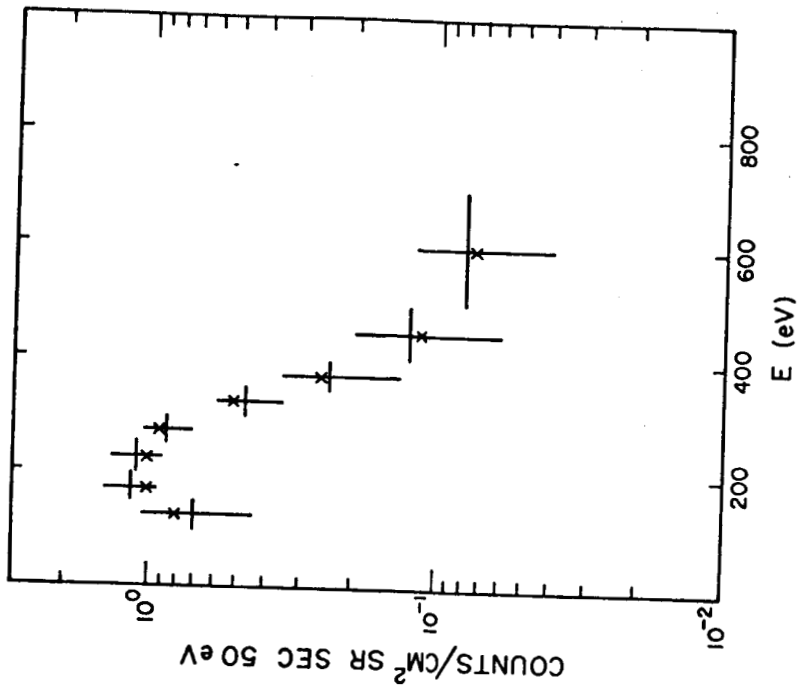

Figure 8

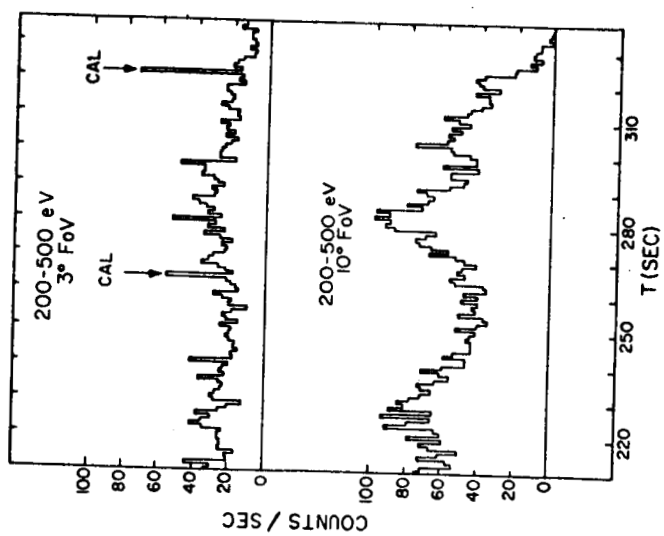

Figure 7

radiative phase of old supernova remnants. A radio feature at $\ell^{II} \simeq 205^{o}$ and $b^{II}+15^{o}$ on Landeker's (1971), 150 MHz map is suggestive of a spur-like feature (Novick, 1974) but a detailed radio map of this region does not seem to support this contention (McKay, Baldwin, 1974). A detailed H_{α} study of this region is in progress (Murdin, Meaburn, 1974). A similar feature in Eridanus does not show a good correlation on the 150 MHz map of Landeker. The spectrum of the bright region in Eridanus appears somewhat harder than the Gem-Mon region based on the relative strengths in the 150-400 eV and 500-1000 eV bands.

This concludes the preliminary results from the Australian expedition. This work was supported in part by NASA contracts NGR 05-002-284 and NGL 05-002-207. Dr. Garmire was supported during part of this work by a John Simon Guggenheim and a Fulbright Fellowship. We would like to thank the sounding rockets division of Goddard Space Flight Center for excellent support, the Australian Weapons Research Establishment and White Sands Missile Range personnel. Mr. J. Vu, J. Coulson and A. Barclay of CIT provided good support for the technical preparation and launching of the experiment.

REFERENCES

Baldwin, J. 1974, (Private Communication).

Bleeker, J. A. M., Deerenberg, A. J. M., Yamashita, K., Hayakawa, S. and Tanaka, Y. 1973, Ap. J. (Letters), 183, L1.

Giacconi, R., Murray, S., Gursky, H., Kellogg, E., Schreier, E., Matilsky, T., Koch, D. and Tananbaum, H. 1974, Ap. J. Suppl., 27, No. 237.

Hill, R. W., Burginyon, G., Grader, R. J., Palmieri, T. M., Seward, F. D. and Stoering, J. P. 1972, Ap. J., 171, 519.

McKay, C. 1974, (Private Communication).

Meaburn, J. 1974, (Private Communication).

Murdin, P. 1974 (Private Communication).

Murdin, P. G., Penston, M. J., Penston, M. V., Glass, I. S., Sanford, P. W., Hawkins, F., Mason, K. and Willmore, A. P. 1974, preprint.

Price, R. E., Groves, D. J., Rodrigues, R. M., Seward, F. D., Swift, C. D. and Toor, A. 1971, Ap. J. (Letters), 168, L7.

Ryter, C., Cesarsky, C. J. and Audouze, J. 1974, preprint.

Schreier, E., Lewison, R., Gursky, H. Kellogg, E., Tananbaum, H., and Giacconi, R. 1972, Ap. J. (Letters), 172, L79.

Vidal, N. V., Wichramasinghe, D. T., Peterson, B. A. and Bessell, M. S. 1974, Ap. J. (Letters), 191, L23.

Wichramasinghe, D. T., Vidal, N. V., Bessell, M.S., Peterson, B. A. and Perry, M. E. 1974, Ap. J., 188, 167.

V) Comet Kohoutek He I Observation

a) Search for Extreme Ultraviolet Radiation from Comet Kohoutek

As a part of Operation Kohoutek, an extreme ultraviolet filter photometer was flown piggy-back on a Johns Hopkins University Aerobee 200 rocket on January 4, 1974, at 1845 MDT. The photometer had been flown previously on two Aerobee 170 experiments 13.063 and 13.064.

The rocket launch was performed successfully, and the photometer performed well throughout the flight. Unfortunately, weight increases reduced the peak altitude significantly compared to the peak altitude which was expected when the project was initiated. As a result, the line-of-sight photoelectric absorption by nitrogen and oxygen was quite severe (0.045% transmission). In addition, possible deviations of the actual atmospheric density profile from the assumed Jacchia (1971) model atmosphere place a large range of uncertainty on the actual EUV transmission. We are

presently in contact with Mr. N. Spencer of Goddard Space Flight Center who will attempt to extract an improved vertical neutral-density profile from Atmospheric Explorer AE-C data. Any improved density profile would then reduce the uncertainty in the transmission correction to the EUV search for helium emission on Comet Kohoutek.

Details of the experiment and the method of data interpretation are given in the enclosed report "A Search for Extreme Ultraviolet Radiation from Comet Kohoutek", by Guenter R. Riegler and Gordon P. Garmire.

Pre-and post-flight calibrations have been performed at the EUV monochromator facility of the Space Sciences Laboratory, The University of California, Berkeley. After the flight, only the detector and the filter were analyzed, since the telescope was damaged upon rocket impact.

b) Study of the Geocoronal EUV Airglow of Helium

The above-mentioned rocket observation of Comet Kohoutek was carried out near twilight. Data recorded prior to and after peak altitude are a valuable addition to the previously available set of helium 584 A airglow data. Other experiments during the past 15 years have been conducted either well in the dayside, or in the nightside of the earth with solar zenith angles larger than approximately 130^{o}. For example, both of our previous 584 A measurements were conducted with solar zenith angles near 130^{o} (see "Observations of the Extreme Ultraviolet Nightglow" by G. R. Riegler and G. P. Garmire, Journal of Geophysical Research 79, January 1, 1974, p. 226-232). The 584 airglow observations conducted during the Comet Kohoutek rocket flight are unique since they were conducted at twilight with solar zenith angle of 110^{o} and at a zenith angle of 90^{o}.

We are presently studying all available rocket-borne helium EUV measurements in an attempt to generate a coherent theoretical multiple-reasonance-scattering model of the 584 A airglow. This study is necessary since the solar line width and line intensity as well as the experimental data used in the previous study by Meier and Weller (1972) were either erroneous or incomplete. The present theoretical calculations use the solar 584 A line widths measured by the University of Colorado and NRL groups, and uses the revised AFCRL/Smithsonian integral line flux measurements. The 584 A model calculations are a collaborative effort with Dr. Gary Thomas, University of Colorado, and Dr. Don Anderson, Naval Research Laboratory.

c) Progress on Detector Fabrication, Electronics etc.

Since the last progress report, our in-house laboratory effort on prototype high-resolution detectors was completed. Drawings for the rocket version have been completed and sent to two manufacturers for quotations. One quote was received, and the other promised within one week.

The electronics system for the microchannelplate detector assembly was outlined. Some interfaces with the Caltech telemetry buffers, timers, low-voltage power circuits etc. were agreed upon. Portions of the MCP electronics system, including the diode array position information encoder, the A/D converter, indicators and bypasses for the ion pump, housekeeping circuits and interchange mechanism drive have been detailed.

An envelope drawing for the position-sensitive proportional counter and the MCP detector system (including electronics) was produced. Layout drawings for the mechanical interchange mechanism and a parts list for the MCP mechanical assembly have been generated.

VI. Vela, Puppis A and Gem-Mon bright patch observations

One of the primary scientific objectives of the 13.063 flight was to make a two dimensional X-ray map of the Vela Supernova Remenant. For basic physical reasons, including time aloft and the number of available maneuvers, this map has limited spatial resolution and hence is composed of cells, with each cell taking the value of the total X-ray intensity from that area of the sky. (See Figure 1). In addition, because of statistical uncertainties, the values associated with each cell are in error. The method previously employed by the X-ray astronomy community to produce these maps could not be made to yield this statisfical error. A new computor program has now been developed and used to process the data from the mission, producing the best possible map (in the maximum likelihood sense) and the statistical error associated with each cell.

The program is a variation of the standard Least Squares Solution of Linear Equations Program, employing a novel method to do the required matrix inversion. This method uses the eigenvectors and eigenvalues of the matrix to find the best inverse, in terms of the information available. The results of applying this program to the data are shown in Figure 1.

Many tests of the program have been made on known distributions. It has been shown to be a very reliable method for producing these maps.

We have also investigated and resolved the problem of finding the minimum size the cells could be, and still be determined by our data. This size is rather larger than previously believed.

The method that has been employed by X-ray astronomers to produce similar maps on other objects has also been used with the data. These results are in qualitative agreement with the results obtained using the new method.

However, the new method produces a substantially better map, as determined by the X^2 criterion.

The X-ray spectrum of the Vela Supernova Remenant has also been produced, and will be presented together with the map of the region.

In addition, the X-ray spectrum of Puppis-A Supernova Remenant has been obtained from three independent detectors. These results are mutually in excellent agreement and will soon be put in a form necessary for publication.

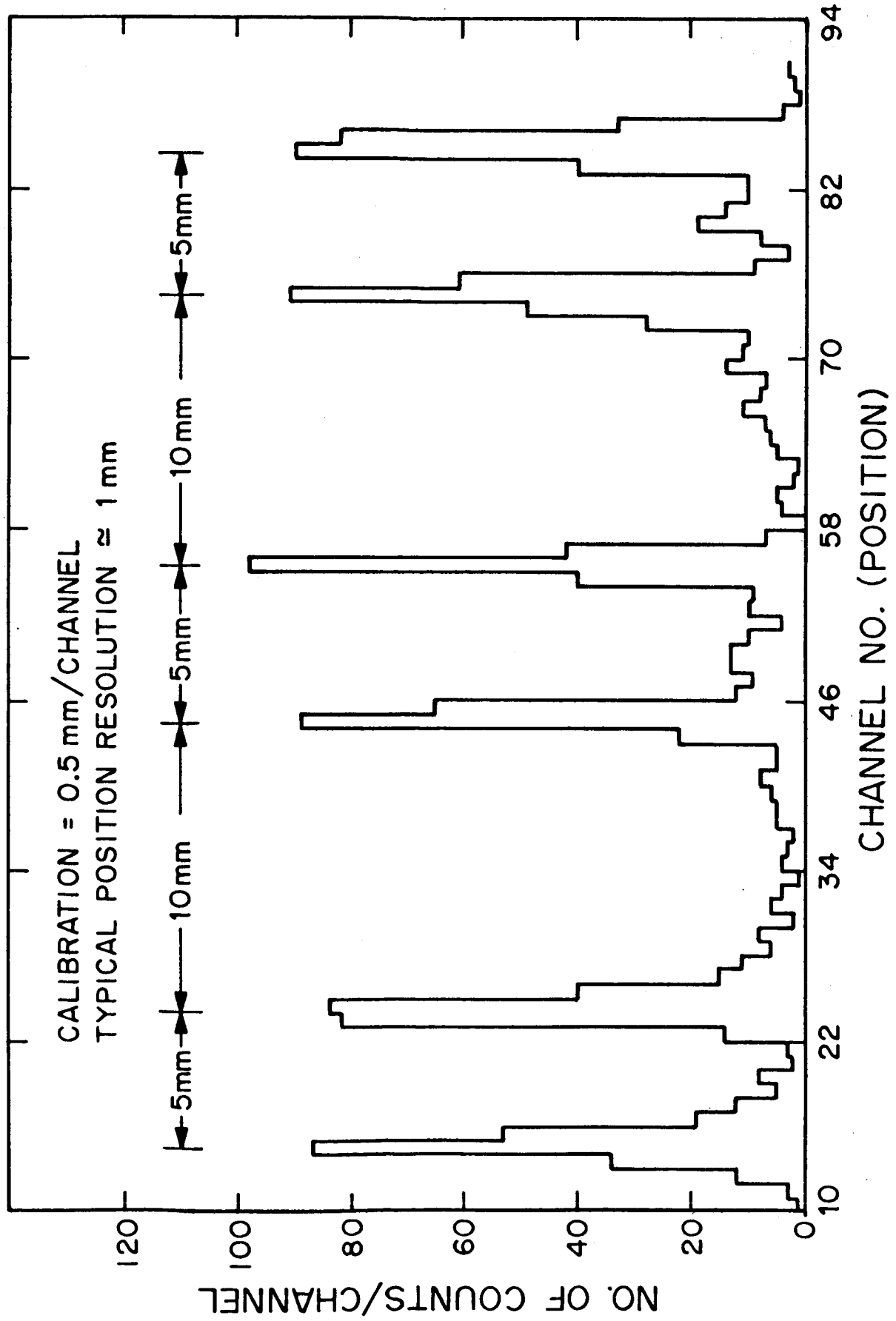
CALIBRATION = 0.5 mm/CHANNEL
TYPICAL POSITION RESOLUTION ≅ 1 mm
5mm
10mm
5mm
10mm
5mm
NO. OF COUNTS/CHANNEL
0
20
40
60
80
100
120
10
22
34
46
58
70
82
94
CHANNEL NO. (POSITION)

Figure 1

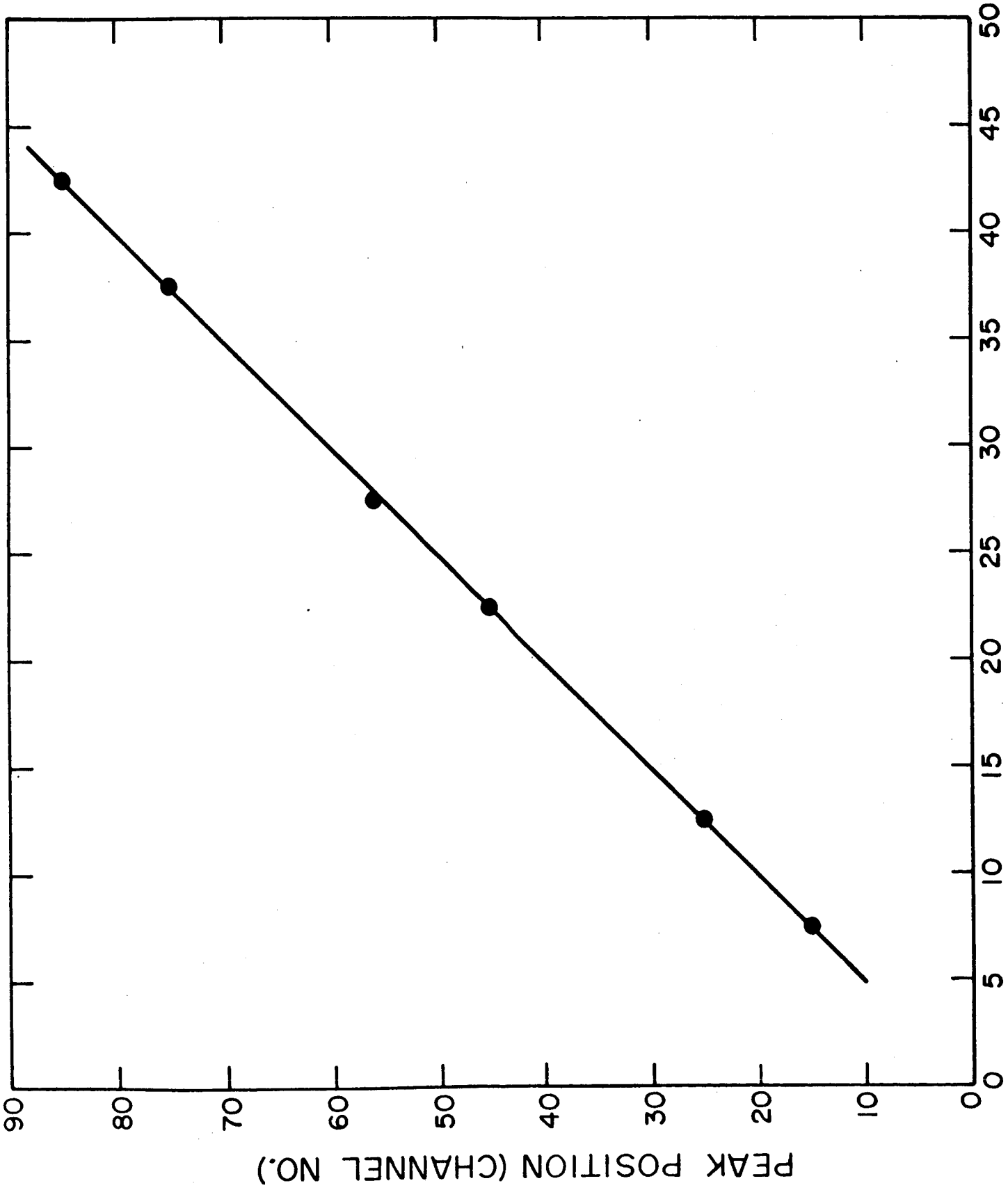
PEAK POSITION (CHANNEL NO.)
90
80
70
60
50
40
30
20
10
0
POSITION (mm)
0
5
10
15
20
25
30
35
40
45
50

Figure 2

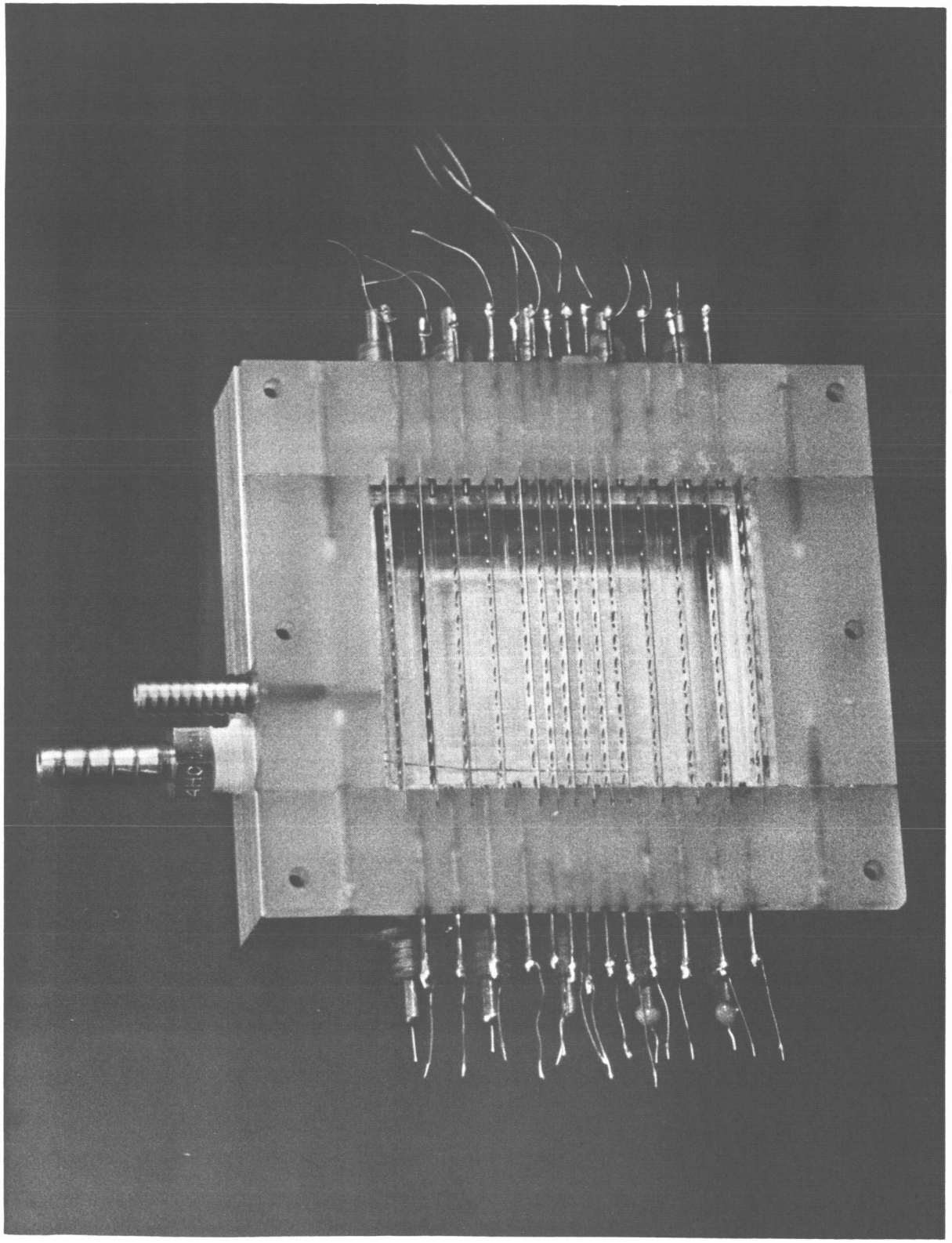

Figure 3

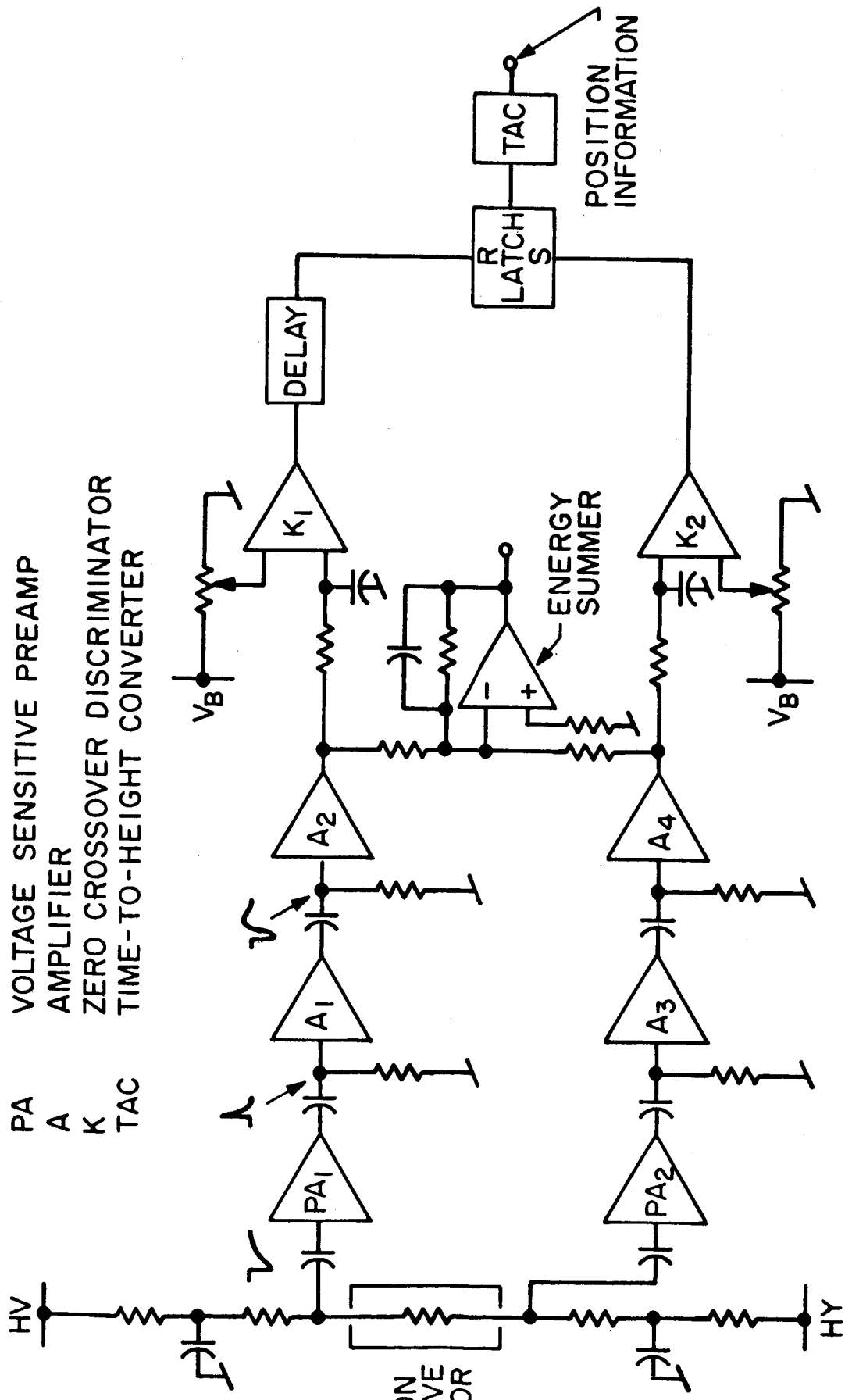
NOMENCLATURE
PA VOLTAGE SENSITIVE PREAMP
A AMPLIFIER
K ZERO CROSSOVER DISCRIMINATOR
TAC TIME-TO-HEIGHT CONVERTER
HV
HY
PA1
PA2
A1
A2
A3
A4
K1
K2
DELAY
R
LATCH
S
TAC
POSITION INFORMATION
ENERGY SUMMER
VB
VB
POSITION SENSITIVE DETECTOR

Figure 4

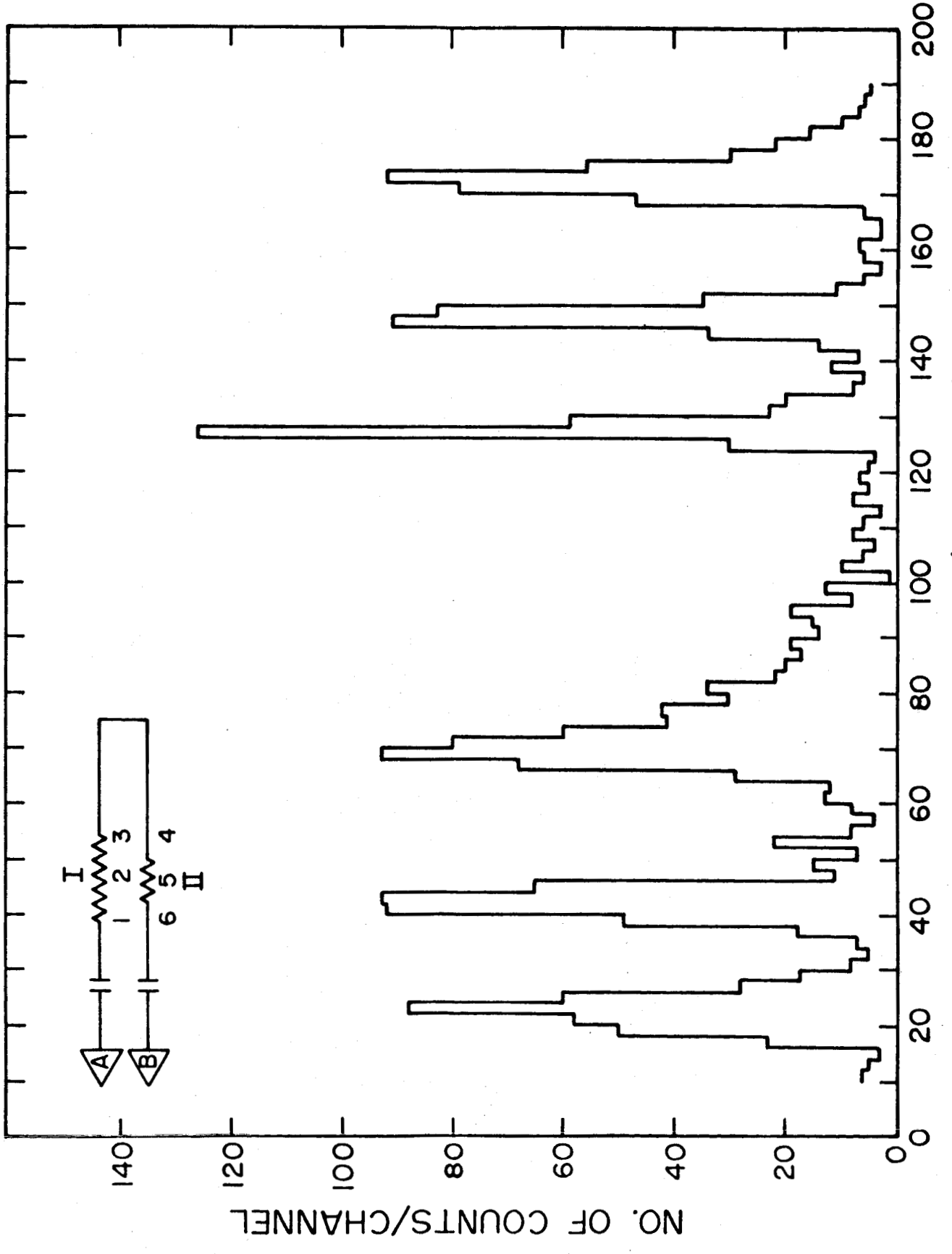
NO. OF COUNTS/CHANNEL
CHANNEL NO. (POSITION)
0
20
40
60
80
100
120
140
160
180
200
I
II
1
2
3
4
5
6
A
B

Figure 5

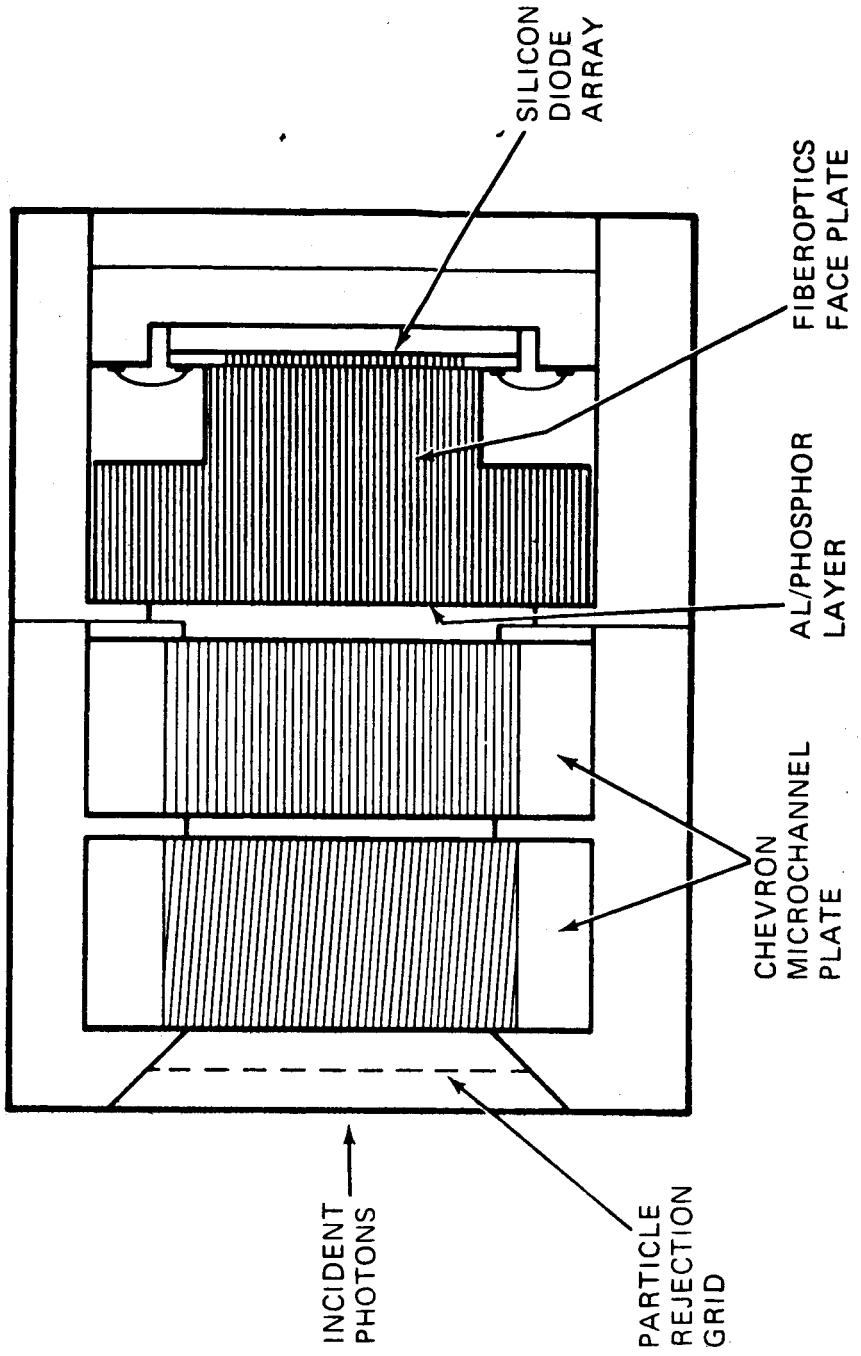

HIGH - RESOLUTION POSITION-SENSITIVE DETECTION SYSTEM

Figure 6

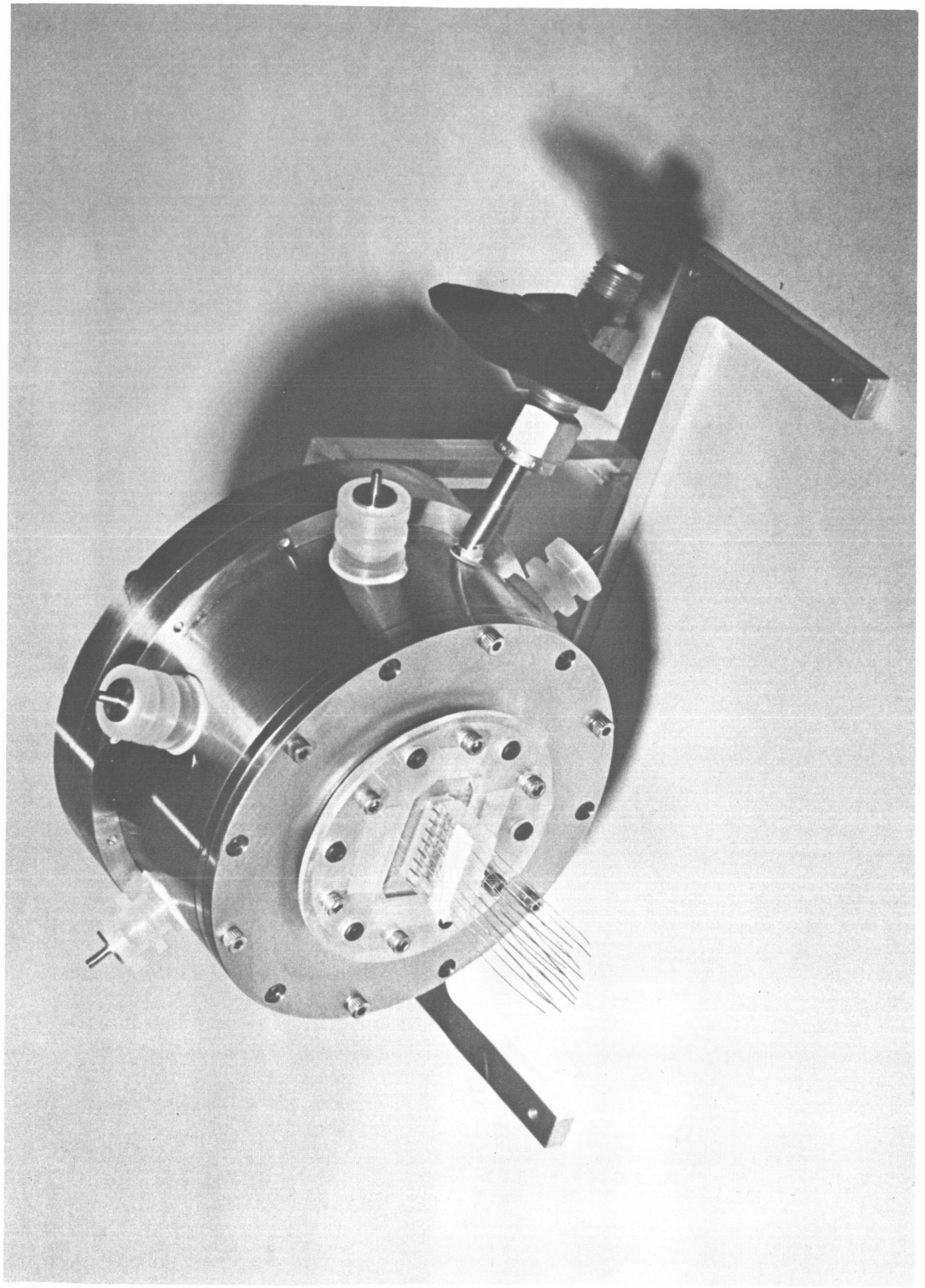

Figure 7

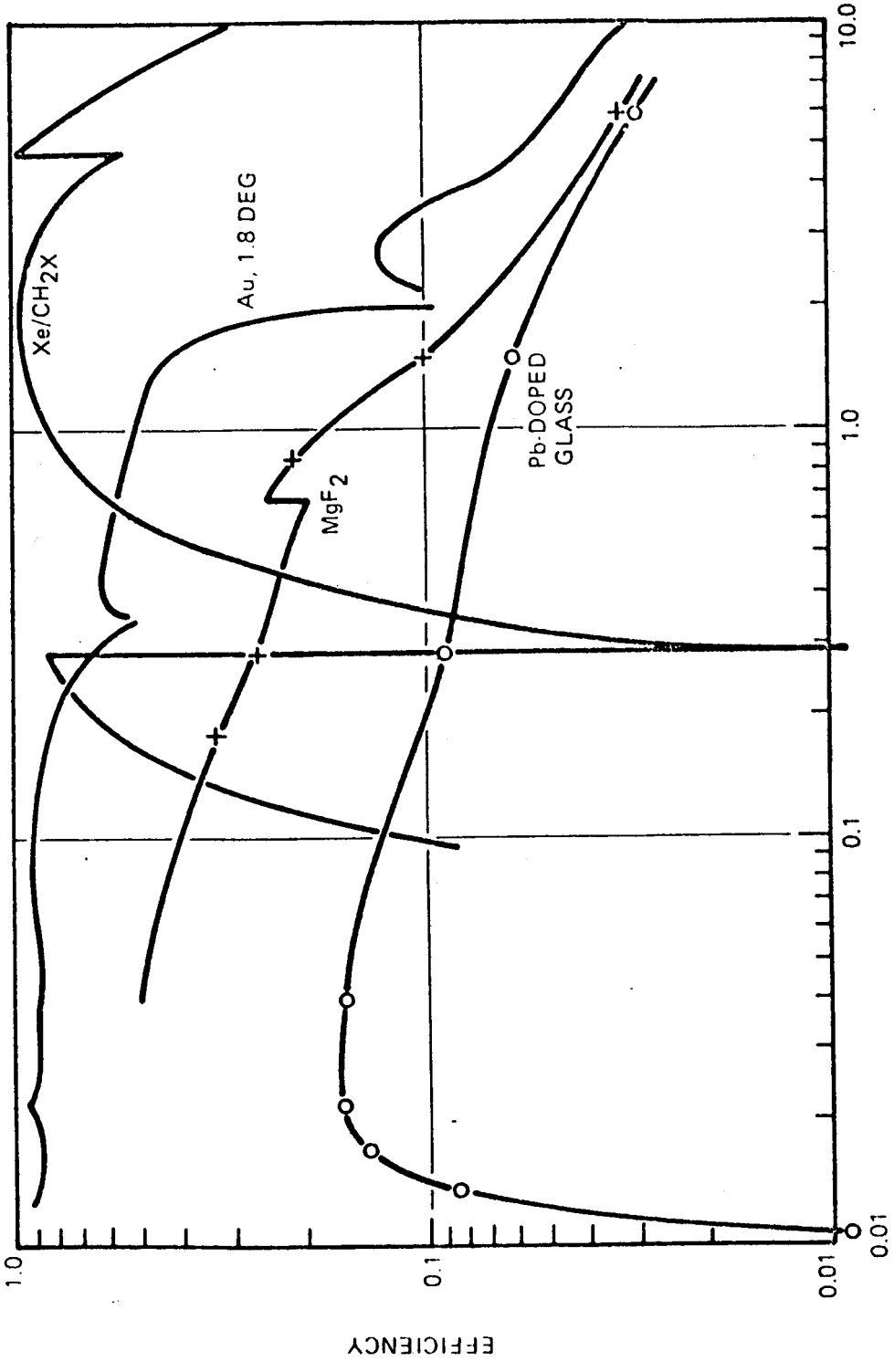

EFFICIENCY OF THE X-RAY TELESCOPE AND DETECTORS

Figure 8

PARABOLOID: $y^2 = p(2w + p)$

$= p(2(x + 2e) + p)$

HYPERBOLOID: $\left(\frac{w - e}{a}\right)^2 - \left(\frac{y}{b}\right)^2 = 1;\ e^2 = a^2 + b^2;\ w = x + 2e$

	INNER PAR./HYP:	OUTER PAR./HYP:
	p = 0.19318156 in.	p' = 0.27962117 in.
	e = 20.00000000 in.	e' = 20.00000000 in.
	a = 19.92314246 in.	a' = 19.88901852 in.
	b = 1.75168326 in.	b' = 2.10403001 in.
X1 = 60.50000000 in.	Y1 = 6.23432535 in.	Y1' = 7.50213590 in
X0 = 50.00000000 in.	Y0 = 5.90000000 in.	Y0' = 7.10000000 in.
X2 = 39.50000000 in.	Y2 = 4.92937576 in.	Y2' = 5.93234767 in.
	$\theta 1 = 0.0318 = 1.824^\circ$	$\theta 1' = 0.0383 = 2.19^\circ$
	$\theta 2 = 0.0924 = 5.296^\circ$	$\theta 2' = 0.1112 = 6.37^\circ$
	$A = 12.7\ in^2 = 82.22\ cm^2$	$A' = 18.4\ in^2 = 119.1\ cm^2$

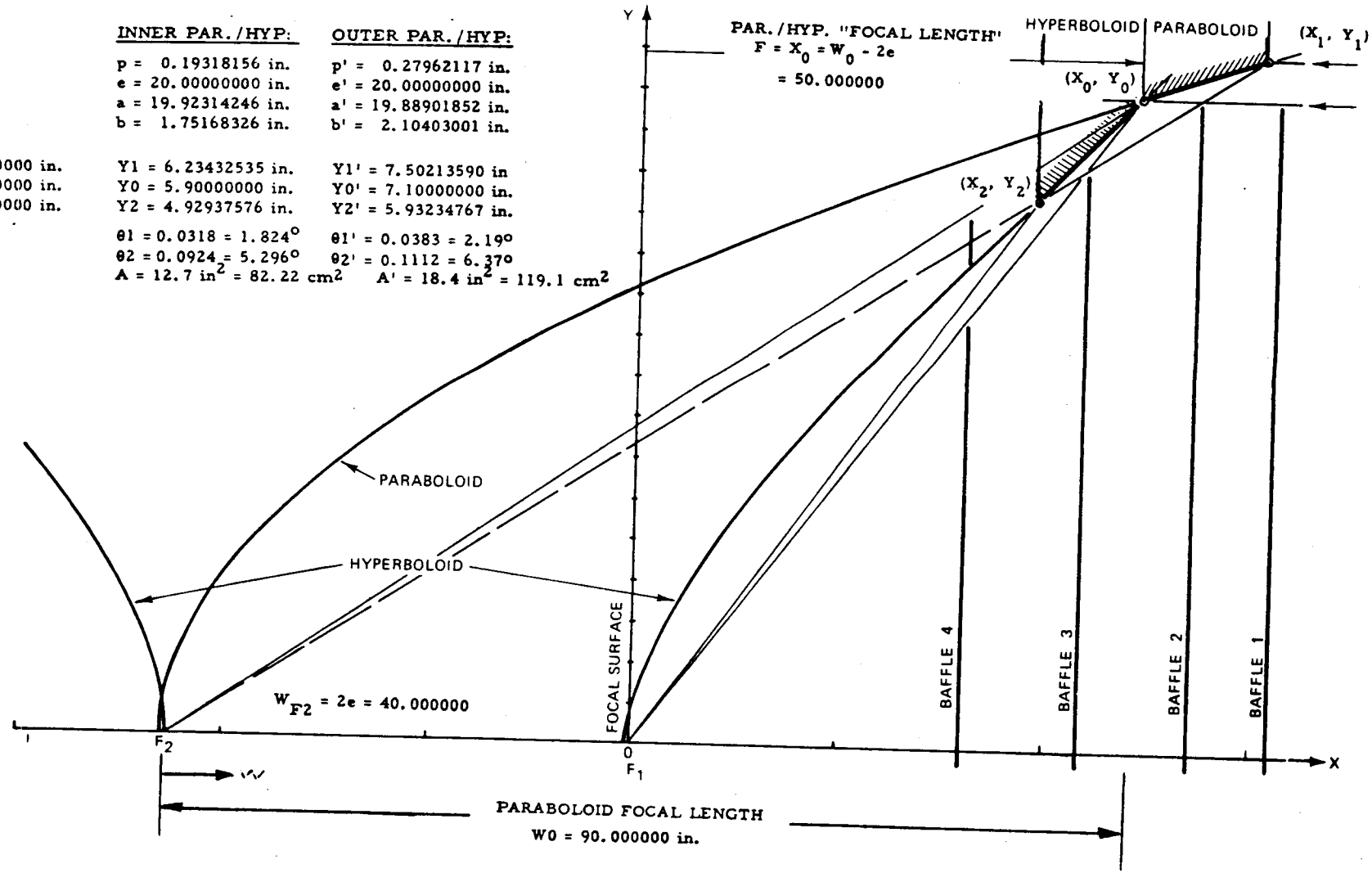

OPTICAL DESIGN FOR THE
ASTROBEE X-RAY TELESCOPE
EXPERIMENT 25.001/2

Figure 9

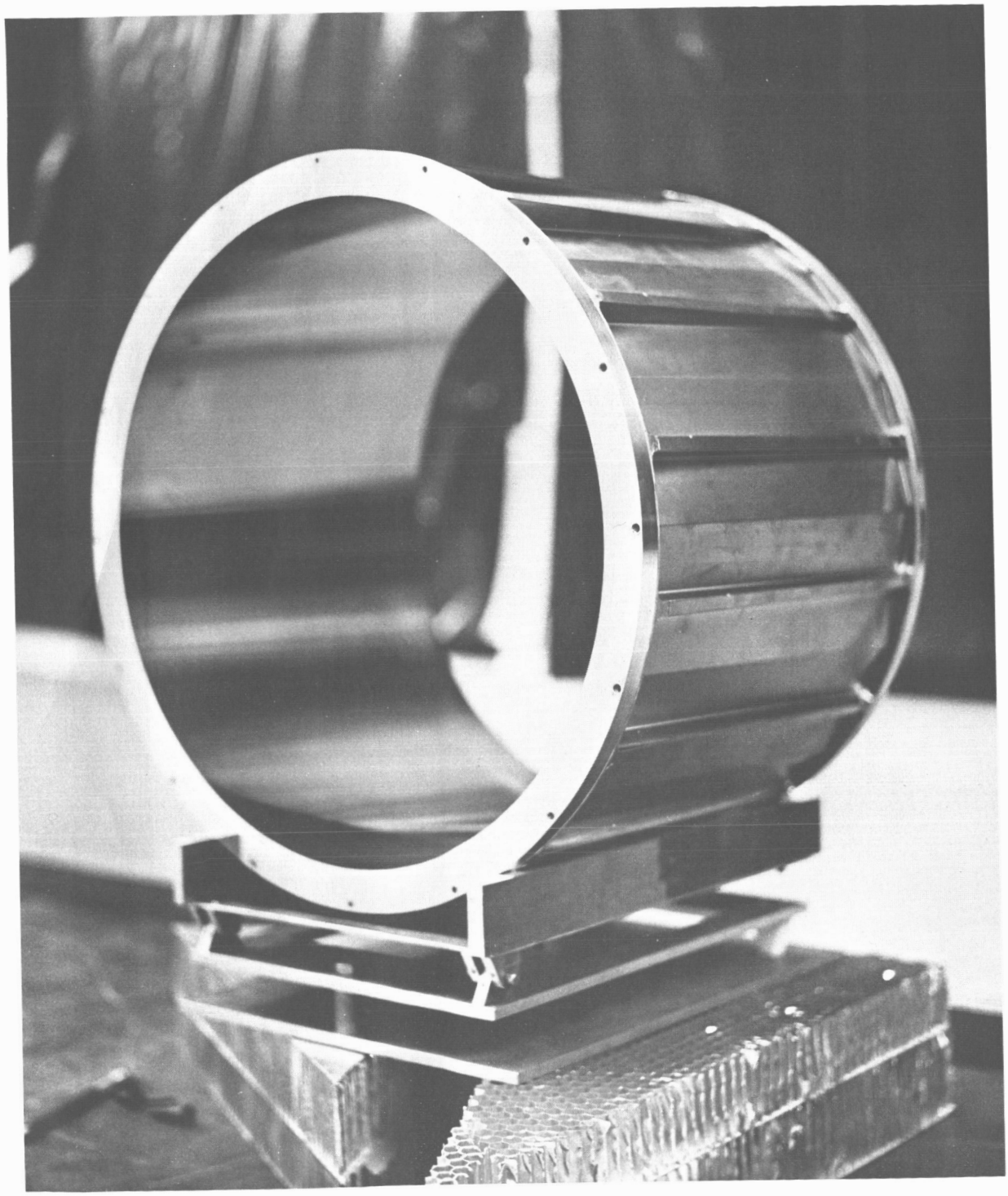

Figure 10